

Challenges and prospects for better measurements of the CMB intensity spectrum

Giorgio Sironi^{a,1,2}

^aPhysics Department, University of Milano Bicocca
Piazza della Scienza 3, Milano, Italy

E-mail: giorgio.sironi@unimb.it

Abstract. Spectral distortions of the Cosmic Microwave Background (CMB) offer the possibility of probing processes which occurred during the evolution of our Universe going back up to $Z \simeq 10^7$. Unfortunately all the attempts so far carried out for detecting distortions failed. All of them were based on comparisons among absolute measurements of the CMB temperature at different frequencies. We suggest a different approach: measurements of the frequency derivative of the CMB temperature over large frequency intervals instead of observations of the absolute temperature at few, well separated, frequencies as frequently done in the past, and, direct measurements of the foregrounds which hinder observations, at the same site and with the same radiometer prepared for the search of CMB distortions. We discuss therefore the perspectives of new observations in the next years from the ground, at very special sites, or in space as independent missions or part of other CMB projects

Keywords: cosmic microwave background, cosmology: diffuse radiation, cosmology: observations

ArXiv ePrint: [:1603.07565 \[astro-ph.IM\]](https://arxiv.org/abs/1603.07565)

¹*in extenso* version of the invited talk presented at CMB@50, Princeton 9-12 June 2015

²retired since Nov.11th, 2011

Contents

1	Introduction	1
2	Expected distortions	2
3	Search of distortions by absolute measurements of $T(\nu)$	4
3.1	Region 1: low frequency, ($\nu \leq 30GHz$)	7
3.2	Region 2: ($30GHz \leq \nu \leq 600GHz$)	8
3.3	Region 3: high frequency ($\nu > 600GHz$)	8
4	A new approach to the search for spectral distortion	8
4.1	Measurements of the frequency derivative of the sky brightness temperature	9
4.2	Contamination from the environment	10
4.3	Foregrounds	11
4.4	Extraction of the CMB signal from the sky signal	12
4.5	Additional requirements of future experiments	14
4.6	Practical system configurations	17
5	Perspectives of new searches of CMB spectral distortions	20
6	Conclusions	21

1 Introduction

Observations aimed at checking the blackbody shape of the CMB spectrum began immediately after the discovery of the CMB by Penzias and Wilson in 1964 [1], but ~ 25 years of efforts were necessary to get sure evidence [2].

According to the most recent evaluations [3] the blackbody spectrum which best fits the CMB spectrum has temperature :

$$T_{CMB} = (2.72548 \pm 0.00057) K \quad (1.1)$$

and maximum of brightness (per unit frequency interval) at:

$$\nu_B = (58.83 T_{CMB}) = 160.3 GHz \quad (1.2)$$

Deviations from a perfect planckian spectrum, the so called *spectral distortions*, are however expected. Produced by injection in the matter radiation mixture of our Universe of energy released by a variety of phenomena which accompany the Universe evolution, they can be used to probe occurrence and properties of these phenomena, going back in time up to $Z \simeq 10^7$, about a week after the Big Bang, well before the decoupling era at $Z \simeq 10^3$, about 300000 years later, when the CMB spectral shape and spatial anisotropies were frozen and got the shape we see today.

But other 25 years elapsed and today, 50 years after the discovery of the CMB, no distortion has been yet discovered, in spite of many attempts and firm belief by the scientific community that distortions must be present.

Origin and shape of distortions are widely discussed in literature (see next section for references), so in the following we give just a brief summary of what we can expect to see. Then we look at the values of the absolute temperature of the CMB measured at different frequencies: comparisons of values obtained at different frequencies is the only method so far used for searching CMB spectral distortions. But all the attempts failed. We suggest therefore a different observational approach: differential measurements of temperature, with continuous frequency coverage and measurements, by the same system in the same area of sky, of the foregrounds which hinder observation of the CMB features. We finally discuss the perspectives of carrying such measurements.

2 Expected distortions

Distortions are triggered whenever the equilibrium of the matter radiation mixture of our Universe is disturbed by energy injections caused by a variety of phenomena, among them particle annihilations, photon and particle production, shock wave dissipation, line emissions etc.. Matter - radiation interactions then smear the original distortions and gradually redistribute the energy over the CMB spectrum (for a complete discussion see for instance Partridge [4] and references therein).

Let's call Z_{inj} the epoch when the energy injection occurred and define

$$\delta T(\nu) = T(\nu) - T_{CMB} \quad (2.1)$$

spectral distortion,

$$A(\nu) = \frac{\delta T(\nu)}{T_{CMB}} = \frac{T(\nu)}{T_{CMB}} - 1 \quad (2.2)$$

distortion amplitude, and

$$\frac{dA}{d\nu} = \frac{1}{T_{CMB}} \frac{dT(\nu)}{d\nu} \quad (2.3)$$

frequency derivative of A, where T_{CMB} and $T(\nu)$ are respectively the thermodynamic temperature¹ of the CMB undistorted spectrum and the thermodynamic temperature effectively measured at frequency ν .

Evolution and frequency spectrum of the above quantities depend on the phenomenon which disturbed the matter-radiation mixture, the epoch Z_{inj} when the phenomenon occurred and the processes of matter-radiation interactions which follow it. These processes are usually characterized by different parameters: Y_{ff} for free-free transitions, μ , the chemical potential,

¹*thermodynamic temperature* $T(\nu)$ is the temperature an ideal blackbody described by the Planck Law should have for producing the brightness $B(\nu)$. It is different from: i) the *brightness temperature* $T_b(\nu) = B(\nu)c^2/2K\nu^2$, frequently used by radioastronomers, obtained assuming the Raleigh Jean approximation instead of the Planck Law to link B and T, therefore

$$T(\nu) = T_b(x_b) \frac{1}{\ln(x_b) + 1} \quad x_b = h\nu/KT_b \quad (2.4)$$

$$T_b(\nu) = T(x) \frac{x}{e^x - 1} \quad x = h\nu/KT \quad (2.5)$$

ii) the *antenna temperature* $T_a = P/(K\Delta\nu)$ where P is the total power which arrives (from sky and environment) to an antenna of effective aperture A_e and total solid angle Ω_a within a frequency bandwidth $\Delta\nu$. Based on Nyquist law, a Raleigh Jeans approximation of the Planck Law, T_a is the brightness temperature of a signal of average brightness $\bar{B} = P/(A_e\Omega_a\Delta\nu)$

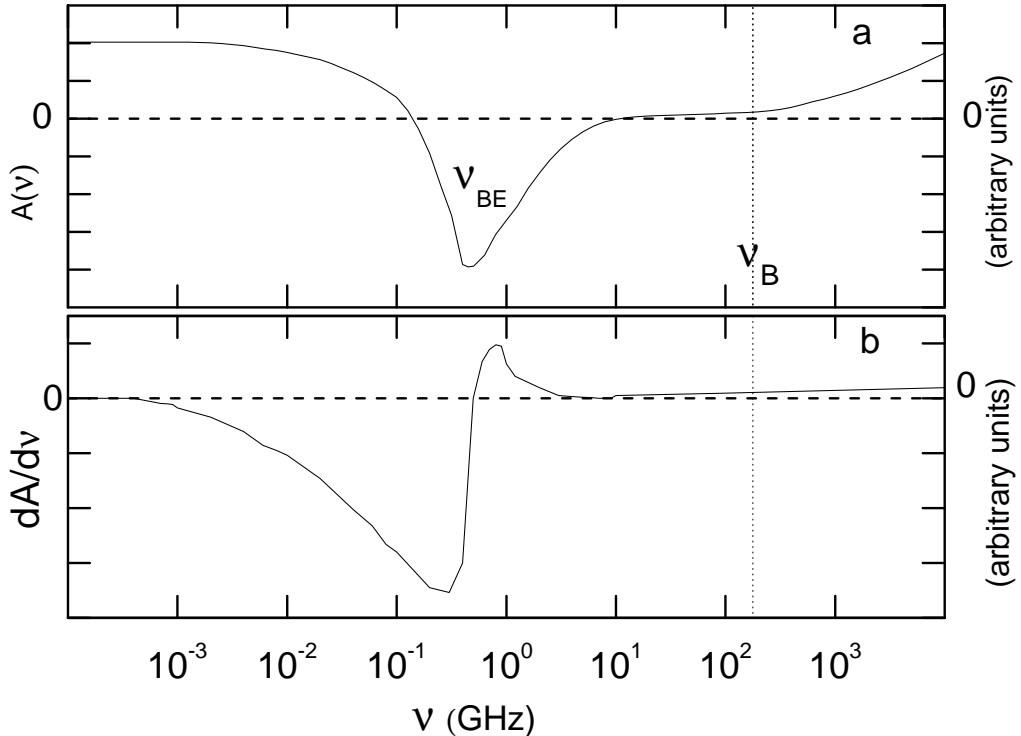


Figure 1. Trend of the frequency profile of a Bose Einstein distortion produced by an energy injection ΔE at a precise epoch $10^4 < Z_{inj} < 10^7$. *Panel a* : Amplitude $A(\nu)$, *Panel b* : Frequency derivative of the Amplitude, *both Panels* : undistorted spectrum (dashed line). $A(\nu)$ depends on Z_{inj} and ΔE , ν_{BE} on the Universe barion density Ω_b . The effective trend of CMB distortions hopefully we will observe probably will be a superposition Bose Einstein distortions triggered by different energy injections at different epochs plus distortions produced by energy injections at $Z_{inj} < 10^4$. $\nu_B =$ frequency of maximum CMB brightness.

for the combination of processes which bring to Bose Einstein instead of Planck Spectra and y for comptonization (see for instance [4, 5] and references therein).

In literature there are many studies (see for instance refs. [6–10]) of the distortions we can expect. Carried out solving analitically and/or numerically diffusion equations, they produced a large collection of possible profiles of $A(\nu)$ versus ν from which it appears that:

i) when $Z_{inj} > Z_{ther} \approx (10^6 - 10^7)$ matter-radiation interactions are so strong and fast that thermalization is obtained almost immediately, a new equilibrium spectrum comes out and distortions disappear. When this is the case the distribution of $T(\nu)$ versus ν is perfectly flat. The only track of energy injections which remains is an increase of the CMB temperature, but we cannot detect it unless we discover an independent source of information which keeps track and bring to us information on the previous value of the CMB temperature.

ii) when $Z_{inj} < Z_{ther}$ the time elapsed between Z_{inj} and now is insufficient to produce complete thermalization so footprints of the original distortions survive and should be observable today in the CMB spectrum.

More precisely

a) if $Z_{inj} > Z_c \approx 10^4$ a Bose Einstein semiequilibrium instead of a Planckian equilibrium spectrum is attained, characterized by a *chemical potential* μ proportional to the energy injection ΔE which triggered the distortion. Detailed frequency profiles of the amplitude $A(\nu)$ of the expected distortions, calculated for different values of Z_{inj} and ΔE can be found in literature (e.g [7]- [9]). All the Bose Einstein distortions have similar frequency dependence of their amplitudes $A(\nu)$ whose general trend, (see fig. 1, panel a), is characterized by:

- an almost flat distribution of $T(\nu)$ versus ν and minimum distortions ($T(\nu) \simeq T_{CMB}$), between few tens and few hundred GHz, the region around ν_B (see eq.(1.2));

- a decrease of $T(\nu)$ below T_{CMB} between few hundred MHz and few ten GHz. As the frequency increases $T(\nu)$ decreases, reaches a minimum (maximum distortion) at $\nu = \nu_{BE}$, then goes back toward T_{CMB} . The amplitude of the maximum distortion is proportional to ΔE and decreases as Z_{inj} increases; ν_{BE} depends on Ω_b , the Universe barion density and slowly increases as Z_{inj} increases. So detecting a Bose Einstein distortion would be extremely informative ;

- at very low and very high frequencies in many cases $T(\nu)$ goes above T_{CMB} .

In the '70, when studies (see for instance [7, 8]) and searches for distortions (see section 3) began, values of $|A(\nu_{BE})|$ in the range $10^{-2} - 10^{-3}$ were not excluded. Today values of $|A(\nu_{BE})|$ greater than 10^{-4} seems improbable and values of $\nu_{BE} \lesssim 1$ GHz are expected.

b) as Z_{inj} goes below $Z_c \approx 10^4$ amplitude, shape and frequency regions where distortions should be observable becomes dependent on the process which triggered the distortion and the epoch when it occurred. There is therefore a variety of expected shapes and amplitudes (see for instance [9]). Among them a special class of distortions characterized by small amplitude and narrow profiles are those produced at $Z_{inj} \sim 1400$, the recombination epoch, by bound-bound and bound-free helium and hydrogen transitions. Usually neglected in the past because the expected amplitudes and profiles are small and narrow compared to other type of distortions, they are now receiving new attention ([11, 12]).

The frequency derivative of $A(\nu)$ provides detailed information on the shape of $A(\nu)$, for instance it allows to pinpoint ν_{BE} in the case of a Bose Einstein distortion or change of slope of $A(\nu)$ profiles. If one day we will arrive to detect distortions, very probably the observed $A(\nu)$ profile will be a superposition of distortions of different types, triggered at different epochs (between $Z \simeq 10^7$ and now), with different values of injected energy. In this case the frequency derivative of the observed profile will help in separating the different type of distortions and recognizing narrow band frequency features combined with wide band frequency features like Bose Einstein distortions.

3 Search of distortions by absolute measurements of $T(\nu)$

All the attempts of detecting CMB spectral distortions reported in literature are based on comparisons of absolute values of $T(\nu)$ measured at different frequencies.

Generally (see for instance [18, 19]) one measures

$$DT(\nu) = T_a(\nu) - T_o(\nu) \tag{3.1}$$

the difference between the radiometer antenna temperature T_a and the brightness temperature T_o of a reference artificial blackbody ².

²Usually an optically thick absorber cooled at the liquid helium temperature, properly shaped to fill completely the radiometer beam. Only Wielebinsky [20] used an astronomical reference source, the Moon dish, of known temperature T_o .

Then, after corrections for the effects (signal attenuation and contamination by system noise) produced by impedance mismatches of radiometer and reference source, DT is added to T_o . This gives the absolute value of T_a from which, after subtraction of T_{for} and T_{env} , the brightness temperatures of the signals produced by the sky foregrounds and the radiometer environment (see subsections 4.3, 4.2 and fig.2) we get the brightness temperature $T_b(\nu)$ of the CMB. Finally $T_b(\nu)$ is converted into the CMB *thermodynamic temperature* $T(\nu)$ and error bars, combinations of statistical and systematics uncertainties of DT, T_o , T_{for} and T_{env} , are added to it.

Fig.3, panel a, shows the frequency distribution of a representative sample of measured values of $T(\nu)$ published before 2002 when the majorities of the observations were made (for the complete list see [21] and references therein). It includes results of the coordinated multifrequency observations made by the White Mt (WM) [22] and South Pole (SP) [23] collaborations. In panel b of the same figure, results of TRIS [19] and Arcade [24], the two coordinated multifrequency experiments made after 2002, are shown.

With the exception of FIRAS ([2, 25]) and the Gush experiment ([26]) which cover continuously extended frequency intervals, the majority of the values of $T(\nu)$ in literature are discrete, isolated, single frequency points, obtained independently by different observers, at different sites, using different radiometers. Only after a few years of observations groups of observers began to coordinate their efforts, measuring the absolute temperature of the same region of sky, at different frequencies, from the same site using similar systems ([18, 22–24] and a common reference source. This way of doing reduced the weight of systematic effects and improved the accuracy of the final results. A further step forward arrived when observers, instead of using the average properties of the foreground and environment signals, included in their experiment ad hoc observations aimed at measuring environment and foreground signal (e.g.[27, 28]).

From fig.3 and all the data in literature it appears that:

i) when the complete set of data is considered there is no evidence of deviations from a flat distribution;

ii) hints, to be confirmed, of deviations can be just glimpsed when results of coordinated observations like White Mt [22], South Pole [23], TRIS [18] and Arcade [24] are plotted separately: for instance an apparent increase of $T(\nu)$ below 3 GHz (see fig.3, panel b) has been suggested by Arcade2 [24], while an opposite trend, a decrease of $T(\nu)$ with frequency, seems to be present in the distributions of the values measured by the WM+SP collaboration. But when error bars are considered both trends look improbable and completely disappear when the results of all the coordinated experiments are merged. This means that systematic uncertainties are still present and we have to go further in reducing them.

iii) the amplitude of the error bars attached to $T(\nu)$ has a frequency dependence which repeats the frequency dependence of the foreground components (see fig.2), decreases when results are from coordinated experiments and is further reduced when observations are made on balloons or in space, where T_{env} is smaller or negligible.

iv) above 600 GHz, in spite of the accuracy of Gush data, results are barely sufficient to confirm that after the peak the brightness spectrum goes down very quickly, as expected in the Wien region of a blackbody spectrum, but we cannot set even poor upper limits to CMB distortions

In conclusion, fifty year after the discovery of the CMB no evidence of CMB spectral distortions has been obtained. Only upper limits can be set [19], ranging between $\sim 10^{-1}$ K at

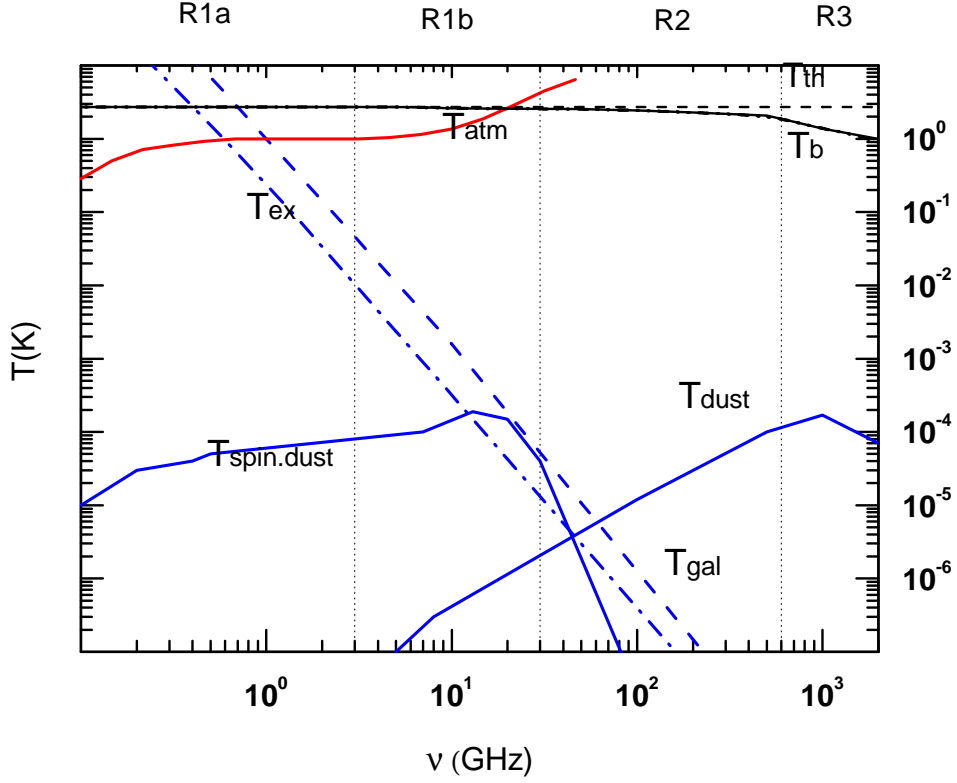


Figure 2. Brightness temperature of contributions to the antenna temperature.
black lines CMB
 T_b : CMB brightness temperature, (T_{th} : CMB thermodynamic temperature, shown for comparison);
foregrounds - blu lines
 T_{gal} : galactic free-free and synchrotron; T_{ex} : blend of unresolved extragalactic sources; T_{dust} : galactic dust; $T_{spin.dust}$: spinning dust; CO contributions are not shown because they are below T_{dust} ;
environment - red line
 T_{atm} : Earth atmosphere (at the zenith, 2000 m a.s.l). The ground contribution T_{ground} is highly dependent on ground profile, antenna side- and backlobes and orientation of the antenna beam therefore it is not shown here.

Foreground (with the exception of the extragalactic signal) and environment are anisotropically distributed, therefore their temperatures and spectra depends on the region of sky observed and the radiometer position. Quoted values and spectra are average quantities.

R1,R2,R3: frequency regions where methods and conditions of observation are similar(see text)

low frequencies and $\sim 10^{-3}$ K at high frequency to the absolute value of the CMB spectral distortion $|\delta T|$, and

$$6 \cdot 10^{-6} < Y_{ff} < 1.3 \cdot 10^{-5}$$

$$|\mu_{BE}| < 6 \cdot 10^{-5}$$

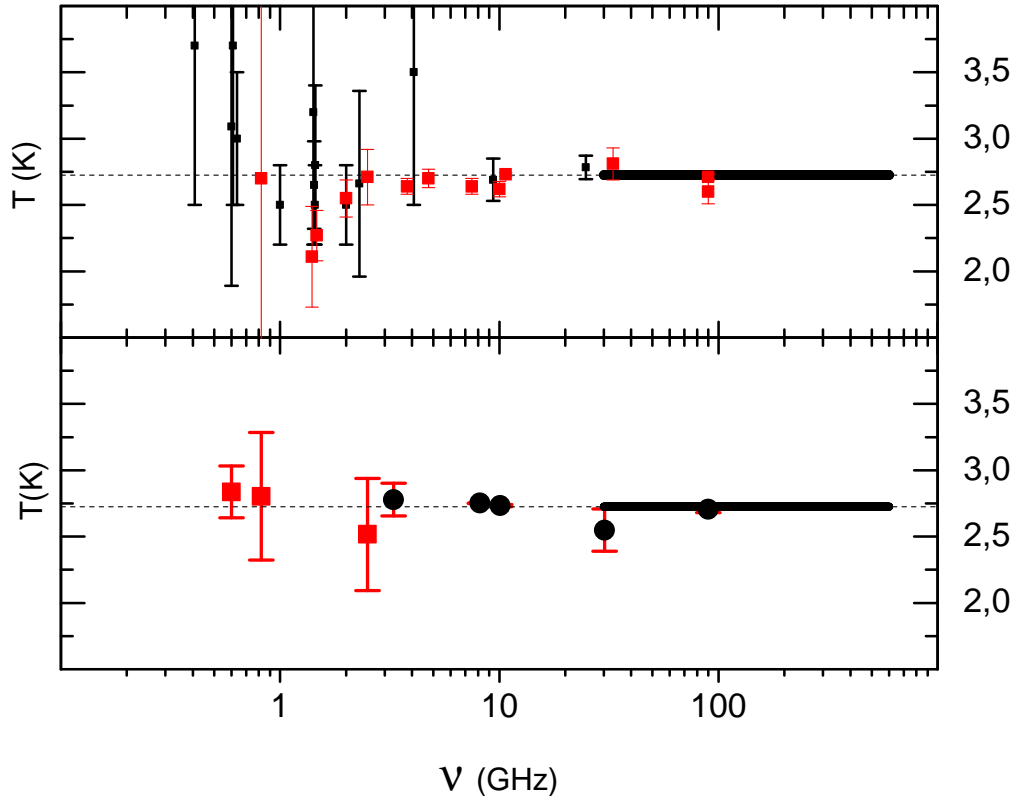


Figure 3. Collection of measured values of the CMB thermodynamic temperature. *Panel a:* old measurements in literature (from the complete list of Burigana and Salvaterra [21]); the results of the coordinated White Mt. [22] plus South Pole [23] observations are shown in red; *Panel b:* recent coordinated observations: TRIS [19] (red squares) and Arcade2 [24] (black dots); *both panels:* FIRAS final results [25] (black horizontal bar) and best value [3] of the undistorted spectrum thermodynamic temperature T_{CMB} (dashed line)

$$|y| < 1.5 \cdot 10^{-5}$$

to the parameters which characterize the interaction processes which affect appearance and evolution of distortions.

Considering the above results, the frequency dependence of foreground and CMB temperatures (see fig.2, 4, 5 and 6) and the different techniques used by different observers, which gradually go from classical radioastronomical methods, dominant at frequencies well below ν_B , to IR methods at $\nu \gg \nu_B$, the observations can be distributed among three frequency regions:

3.1 Region 1: low frequency, ($\nu \leq 30$ GHz)

All the results are single frequency measurements obtained using resonant antennae coupled to low noise radio receivers. Belong to this region: i) the first detection of the CMB by Penzias

and Wilson [1], ii) the first evidence by Howell and Shakeshaft [29] that the low frequency spectrum of the just discovered CMB has a ν^2 frequency dependence of the brightness, iii) sets of coordinated measurements made at White Mt. [22], South Pole [23], Campo Imperatore [18] and at balloon altitude [24]. In region 1 the CMB brightness temperature is gradually covered by the galactic diffuse emission when frequency goes below ~ 1 GHz and by the atmospheric signal when goes above 10 GHz (at sea level). Therefore it may be convenient to split region 1 between subregion 1a - ($0.3 \leq \nu(\text{GHz}) \leq 3$) and subregion 1b - ($3 \leq \nu(\text{GHz}) \leq 30$). The region below 0.3 GHz has not been considered and probably will continue to be neglected because here the foregrounds overcome the CMB by orders of magnitude.

3.2 Region 2: ($30\text{GHz} \leq \nu \leq 600\text{GHz}$)

It includes single frequency observations and measurements with continuous frequency coverage made respectively with antennae coupled to etherodyne systems and radiation concentrators coupled to bolometric detectors [30].

In region 2 foregrounds are small compared to the CMB while atmospheric effects are so important that ground based observations would be impossible were not for two windows at 30 and 90 GHz, used for instance by the White Mt. and South Pole Collaborations. All the remaining observations are from stratospheric balloons and in space.

To Region 2 belong also measurements of $T(\nu)$ at few precise frequencies made studying the excitation temperature of optical lines of CN and other molecules in interstellar space (see review by Partridge [4] and references therein).

3.3 Region 3: high frequency ($\nu > 600\text{GHz}$)

Here absorption and emission by the earth atmosphere are so large that only observations from balloons and in space are possible.

Radiometers, very similar to IR and optical systems, with filters to get the radiation spectrum, can be so small and compact they can be accommodated even in the limited volume available on sounding rockets (on rockets however the observing time is very short and engine exhausts must be added to the list of possible contaminants of the sky signal). In Region 3 observations of the CMB are hindered by the foreground created by dust.

4 A new approach to the search for spectral distortion

The FIRAS accuracy ($\sim 5 \cdot 10^{-3}$ K/(frequency bin)) is the highest so far achieved by absolute measurements but was still insufficient to recognize distortions even integrating over the (30-600 GHz) frequency interval covered by the experiment. Because at FIRAS frequencies foregrounds are small compared to CMB (see figs.4 and 5) and environment contamination was practically absent because observation were made in space, we conclude that the FIRAS accuracy is entirely set by the quality of radiometer and reference source.

Getting better levels of accuracy for new experiments and extending them outside the FIRAS frequency window means not only improving the evaluation of T_{for} and T_{env} , but improving the hardware and reducing error bars, especially systematics among the hardware systems and sub-systems used to carry on the observation, their scales of temperature and the zero levels of these scales. The elimination of systematics, or at least their drastic reduction, can be immediately obtained if we decide to carry on differential, instead of absolute, measurements of temperature.

The advantages of differential measurements are confirmed by: i)the positive results they brought to the search of CMB anisotropy and polarization where accuracies of few part on 10^6 are now common and efforts to reach and overcome a few part on 10^9 are underway (see for instance [13] and references therein); ii)the plans of using them also for other type of observations like studies of the 21 cm line in distant galaxies [14] or the Zeeman effects [15] or the search of the global signal produced by the blend of the hydrogen 21 cm line in sources at redshift $Z \simeq 6$ ([16, 17])³.

We suggest therefore, as we did in the past [31]), that to get better possibilities of detection, new searches for CMB distortions are made:

- i)measuring the frequency derivative of $T(\nu)$ instead of its absolute temperature;
- ii)covering continuously the CMB frequency spectrum or large parts of it (It will make easier recognizing trends and detecting narrow features);
- iii)including direct measurements of environment and foreground contributions, by ad hoc observations.

4.1 Measurements of the frequency derivative of the sky brightness temperature

Let's have a differential system which measures the difference of temperature

$$\begin{aligned}\Delta T_b(\alpha, \delta; a, z; \nu) &= T_b(\alpha, \delta; a, z; \nu_2) - T_b(\alpha, \delta; a, z; \nu_1) = \\ &= \Delta T_b^{CMB}(\nu) + \Delta T_{for}(\alpha, \delta; \nu) + \Delta T_{env}(a, z; \nu)\end{aligned}\quad (4.1)$$

between the brightness temperatures of two signals collected simultaneously at frequencies $\nu_1 = \nu - (\Delta\nu/2)$ and $\nu_2 = \nu + \Delta\nu/2$ with $\Delta\nu = (\nu_2 - \nu_1) \ll \nu = (\nu_1 + \nu_2)/2$ by a radiometer beam aimed at a point on the sky of celestial and horizon coordinates (α, δ) and (a, z) .

Here ΔT_b^{CMB} , ΔT_{for} and ΔT_{env} are the variations of brightness temperature of CMB, foregrounds and environment. Subtracting ΔT_{for} and ΔT_{env} (see next section) we get $\Delta T_b^{CMB}(\nu)$ which is then converted into variations of the CMB thermodynamic temperature (see eqs(2.4) and (2.5) and ref.[10]) by

$$\Delta T(\nu) \simeq \Delta T_b^{CMB}(\nu) \frac{(e^x - 1)^2}{x^2 e^x} \quad x = h\nu/KT_{CMB}, \quad (4.2)$$

Because (see (2.1) and(2.2))

$$\frac{dT(\nu)}{d\nu} = \frac{d}{d\nu}[\delta T(\nu)] = T_{CMB} \frac{dA}{d\nu} \simeq \frac{d\Delta T(\nu)}{d\nu}. \quad (4.3)$$

numerical integration of a distribution of measured values of $dT(\nu)/d\nu$ will give

$$\delta T(\nu) = T(\nu) - T_{CMB} = T_* + \int_{\nu_*}^{\nu} \frac{\partial T}{\partial \nu} d\nu - T_{CMB} \simeq \sum_{\nu_*}^{\nu} \Delta T(\nu_i) \quad (4.4)$$

$$A(\nu) \simeq \frac{1}{T_{CMB}} \sum_{\nu_*}^{\nu} \Delta T(\nu_i) \quad (4.5)$$

³the shape of that feature for many aspects is similar to the shape of the Bose Einstein distortion, but the expected amplitude, (about -100 mK), is higher and occur at about 70 MHz, well below ν_{BE} , in presence of a much higher foreground level.

where ν_* is a frequency where (see fig. 1) the distortion amplitude is very close to 0 so $T(\nu_*) \simeq T_{CMB}$.

Notice that:

i)the differential approach do not improve nor worsen the evaluation of foreground and environment contributions;

ii)being the CMB a monopole, the choice of the point on the sky where to look for $\Delta T(\nu)$ would be independent of (α, δ) and (a, z) where not for ΔT_{for} whose intensity depends on the celestial coordinates of the point where measurements are made and $\Delta T_{env}(a, z; \nu)$ whose importance depends on the horizon coordinates of the radiometer beam.

4.2 Contamination from the environment

This type of contamination is maximum when observations are made on the Earth or close to it, (e.g. on balloons). It includes:

a)atmospheric absorption and emission (see fig. 2). Detailed calculations of T_{atm} , the temperature of the atmospheric signal, its dependence on the elevation of the observing site and the thickness of Earth atmosphere crossed by the radiometer beam and its frequency spectrum are available in literature (e.g. [32] and references therein). They allows to decide immediately if observations at a given frequency can be made from the ground or require stratospheric balloons or space systems.

Because the effective value of T_{atm} depends also on the weather conditions and the position of the observing site to get accurate values, whenever possible, T_{atm} must be measured, usually by zenith scan methods (e.g. Partridge [27]).

Having the temperature of the atmospheric emission the absorption coefficient, necessary to work out the CMB signal corrected for the absorption by the Earth atmosphere, is immediately obtained

$$r \simeq \frac{T_{atm}^{phys} - T_{atm}}{T_{atm}^{phys}} \simeq \frac{240 - T_{atm}}{240} \quad (4.6)$$

where $T_{atm}^{phys} \simeq 240K$ is the average physical temperature of the Earth atmosphere.

b)ground emission. Similar to the signal of a blackbody at ~ 300 K which surrounds the radiometer up to the horizon level, it is collected by the back- and side-lobes of the radiometer beam. The resulting temperature T_{ground} of this signal depends on: i)ground profile above the horizontal plane, ii)level of antenna side- and back-lobes, iii)horizontal coordinates of the antenna beam axis. Practically frequency independent, its value can be controlled surrounding the radiation collector with apodized (to reduce diffraction) reflecting screens.

c)radiointerferences at various frequencies. By-products of human activities, they arrive from the horizon of the observing site and from Earth satellites. Once again they can be reduced by proper sets of screens and frequency filters.

d)emission from close astronomical objects, *in primis* Sun, Moon and, when observing from space, the Earth.

To get T_{env} and ΔT_{env} the radiometer beam shape, measured at a test range paying special attention to the levels of back- and side-lobes, is convolved with the space distribution of the signals from the ground, close astronomical objects, sources of radiointerferences and atmospheric emission.

The importance of T_{env} decreases when observations are made on balloons and go to zero in space except for radiointerferences and contributions from close astronomical objects, which have to be carefully screened.

4.3 Foregrounds

Foregrounds are a superposition of diffuse emission of galactic and extragalactic origin produced by different mechanisms whose relative importance varies with frequency and the sky regions crossed by the line of sight. The extragalactic component is isotropically distributed, while the distribution of the galactic foregrounds is anisotropic and reflects the underlying structure of the Milky Way.

The most important sources of foregrounds are (see fig.2):

1)Free-free or thermal bremsstrahlung process.

Produced by interactions of free electrons with protons and ions of a partially ionized medium, it gives rise to emission from, and absorption in, the region where the electrons and protons move. The brightness temperature of the emission spectrum is characterized by a constant value T_{ff} at $\nu < \nu_o$ and a power law $\nu^{-2.1}$ frequency dependence at $\nu > \nu_o$, ν_o being set by the densities of free electrons and protons in the medium.

In the interstellar medium $\nu_o \lesssim 1$ MHz, $T_{ff} \simeq 100$ K while absorption of the radiation which crosses it becomes important below few MHz.

2)Synchrotron emission from the interstellar medium.

Produced by the interactions of the cosmic ray electrons with the galactic magnetic field, its brightness temperature has a power law $\nu^{-\alpha}$ frequency dependence (see fig. 2), with spectral index α , (directly measured by radio astronomers and/or extrapolated from the energy spectrum of the cosmic ray electrons, with few per cent error bars), goes from about 2.4 for $0.01 \lesssim \nu \lesssim 0.5$ GHz to 2.8 around 10 GHz and about 3.1 at higher frequencies. Below 10 MHz absorption by the interstellar medium comes in gradually bringing α to zero and negative values below 1 MHz. The variations of α take over smoothly, over frequency intervals whose amplitude and central value depend on the regions of the Milky Way crossed by the line of sight (e.g. [33–36]).

Except at frequencies below few MHz where absorption by the interstellar medium begin to appear, the synchrotron signal is always dominant on the free-free signal.

It can be partially polarized (e.g. [37, 38] and references therein) and disturbs primarily observations of the Raleigh Jeans portion of the CMB spectrum.

3)Blend of unresolved extragalactic radio sources. Isotropically distributed, has a power law frequency spectrum similar to, and brightness temperature one or two orders of magnitude weaker than, the galactic synchrotron (see fig.2). It has been studied by various authors (e.g. [39] and references therein) combining the observed counts of the radiosources (the so called log N - log S plots) at various frequencies.

4)Emission from dust present in the interstellar medium, in clouds and their blend. Its emission spectrum is a modified blackbody spectrum (see fig. 2) at ~ 20 K. It can be partially polarized [40, 41] and affects primarily observations in the Wien portion of the CMB spectrum.

5)Emission by spinning dust grains. Its existence has been suggested to explain an apparent increase of the galactic synchrotron between 20 and 70 GHz, the so called Anomalous Microwave Emission [42, 43].

6)CO line emission associated to dust regions [44].

With the exception of the component of extragalactic origin, frequency spectra, relative weights and spatial distributions of the foreground components and their sum T_{for} depend on the underlying structure of the Galaxy and vary as the radiometer beam moves on the sky. So values and spectra of foreground components shown in fig.2, their sum T_{for} and the the ratio T_b^{CMB}/T_{for} between the brightness temperature of CMB and foreground, shown in fig.4, are not effective but average values. The same is true for $dT_{for}/d\nu$ and $\Delta T_b^{CMB}/\Delta T_{for}$, the ratio between the frequency derivatives of T_b^{CMB} and T_{for} , shown in fig.5. The above ratios are sorts of signal (CMB) to noise (foreground) ratios, which can be useful, when we are preparing absolute measurements of temperature, to decide where the CMB is dominant, comparable or buried in the noise, but are insufficient for getting accurate estimates of the contributions to the sky temperature at a given point on the sky.

For measurements of the CMB distortions more convenient quantities are the ratio between the distortion $\delta(\nu) = T_{CMB}(\nu) A(\nu)$ and the signal $T_{for} + T_b^{CMB}$ which hinders the detection of distortions. It is shown in fig.6 assuming for $A(\nu)$ the amplitude of the Bose Einstein distortion shown in fig.1 and $|\delta(\nu)|_{max} = 10^{-4}$ K. Fig.7 gives frequency spectra and average values of $\Delta(\delta(\nu))/\Delta(T_{for} + T_b^{CMB})$ and $d(\delta(\nu))/d\nu$. Once again they are average values which can be very different from the effective values we should observe at a given point on the sky, not only because T_{for} is anisotropically distributed, but also because the amplitude $A(\nu)$ of the distortion we hope to detect one day very probably is a superposition of different types of distortions triggered by different energy injections which occurred at different times, with a trend more structured than fig.1 distribution.

4.4 Extraction of the CMB signal from the sky signal

To disentangle the components of $\Delta T_b(\alpha, \delta; a, z; \nu)$ (see eq.(4.1) and get $\Delta T_b^{CMB}(\nu)$ average values like those plotted in fig 2 and fig.4 to 7 are insufficient. Effective values and precise frequency spectra are necessary. They which can be obtained only from true maps of $\Delta T_b(\nu)$ in a region of sky centered on the point of celestial coordinates (α, δ) where we want to look for CMB distortions with an accuracy at least comparable to the distortion we want to detect, i.e. $+/- 10^{-4}$ K or better.

In literature there are maps of $T_b(\nu)$, which combined with the frequency dependence of the various components of the sky signal, we can to use for calculating ΔT_b . They cover extended regions of northern and southern sky and were prepared in different years, (by the '60 onward), by different observers, at different ground observatories using different systems ([28] and references therein). But only at a few, low, frequencies it was possible to combine them and prepare maps of the full sky (e.g. [37, 45–48]). The situation changed over the last decade when full sky maps of the foregrounds at high frequencies began to arrive from space experiments [49]. Added to the ground observations they now form a large data set which has been used to produce Global Sky Models (GSM) of the diffuse emission of Galactic origin ([16, 50]) and a set of 29 complete maps of the diffuse radiation (5° angular resolution) distributed between 10 MHz and 5 THz is now available ([50]). But the final accuracy of the temperature measurements is very far from the desired accuracy. According the authors [50], the most recent GSM model has in fact a predictive accuracy ranging between 5% and 15% at most frequencies, 2% accuracy at frequencies where the CMB is dominant, and an overall amplitude offset $\lesssim 15\%$. Moreover many of the above maps, especially at low frequencies, there include areas which have never been observed. Here structure and temperature distribution have been obtained extrapolating the trend of the signals measured in nearby areas and/or at other

frequencies. Therefore in these regions the maps cannot account nor exclude the existence of local features which may affect the search for CMB distortions. 1

So foreground and environment contributions to eq.(4.1) cannot be obtained from data in literature and/or simple calculations. We have to measure them. The best way of getting them and separating the various contributions to eq.4.1 is:

i)mapping $\Delta T_b(\alpha, \delta; a, z; \nu)$ in an area around the point where we want to look for CMB distortions (for measurement of the CMB absolute temperature we should have to map $T_b(\alpha, \delta; a, z; \nu)$, at frequency intervals regularly distributed inside the frequency interval we want to explore;

ii)modelling $\Delta T_b(\alpha, \delta; a, z; \nu)$.

For the foreground a model can be prepared considering the properties of the foregrounds we saw before, or derived from the algorithms of the GSM models in literature, and the known properties and structures of our Galaxy in the mapped area. ΔT_{for} and the relative weights of the foreground components at the center of the map can be free parameters.

The model of the environment signal, which depends on the structure and position of the observing site and the horizontal coordinates of the radiometer beam, can have ΔT_{env} and the relative weights of the environment signals can be free parameters;

iii)best fitting model and maps at each frequency will give $\Delta T_b^{CMB}(\nu), \Delta T_{for}(\nu)$ and $\Delta T_{env}(\nu)$;

The computation procedure, far from simple, can be implemented in different ways. They can go from straightforward calculations based on classical methods of bestfitting to very sophisticated methods of model optimization. The choice will depend also on the characteristics of the sky area where observations are going on and the importance of the environment signals. Examples of procedures successfully used for searching weak CMB signal buried in high level of noise like anisotropies at different angular scales or CMB polarization can be found in literature ([51, 52]. Liu et al. [16] suggest a method for extracting from the foregrounds the monopole signal produced by the 21 cm line in galaxies at $Z \gtrsim 6$, expected at frequencies close to 70 MHz, with a shape similar to the feature at $\nu_{BE} \simeq 300$ MHz of a CMB Bose Einstein distortion. The Liu procedure offers the possibility of evaluating the sensitivity one can hope to reach when we plan an experiment, but for application to the search of CMB distortions must be adapted to higher frequencies, and wider frequency regions, with a different composition of the foregrounds (see fig.2).

Whatever the procedure of data reduction one decides to use the extension of the area to be mapped must be:

i)sufficient to provide a number of independent samples large compared to the number of the free parameters we will use to describe foreground and environment signals,

ii)sufficiently small to guarantee that in the mapped region the variations of foreground and environment signals are regular and smooth.

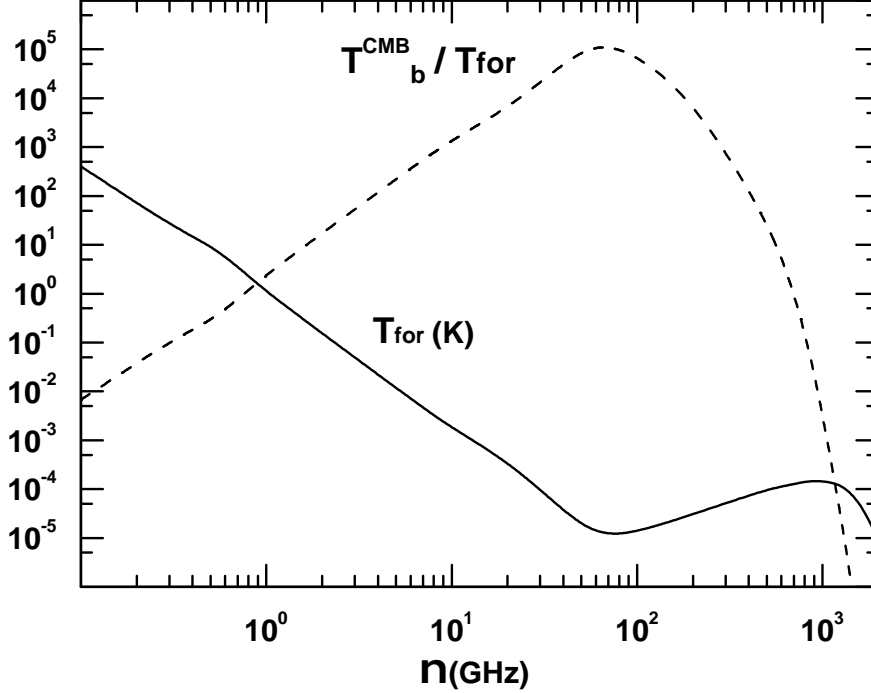


Figure 4. Average behaviour of T_{for} and T_b^{CMB}/T_{for} frequency spectra and values. Their effective values and spectra depend on the region of sky one is observing

4.5 Additional requirements of future experiments

When planning a search for CMB distortions the first step will be looking for sky regions where foregrounds are minimum and vary in regular way.

Then, if observations are from ground observatories additional requirements, important to minimize T_{env} , are: radioquiet site, low horizon profile, high altitude, dry region, latitude close to declination of the regions of sky to be observed.

When these conditions are satisfied we can go on measuring the frequency derivative of $T_b(\nu)$ at regularly distributed points (separated by $\Delta\theta_o$, the radiometer half power beamwidth, in right ascension and declination) around the point selected for the search of the CMB distortion. The procedure is repeated at different frequencies separated by $\Delta\nu_o$, the radiometer frequency resolution, between the minimum and maximum value of the frequency window to be explored

Other requirements are:

- i) radiometer with a well shaped, circular beams, low side- and back lobes (-60 dB), Half Power Beam Width $\Delta\theta_o$.
- ii) possibility of detecting linear polarization at the 0.1% level, a foreground signature;
- iii) sky area to be mapped: free of peculiar features, like the North Galactic Spur ([53]) or the Galactic Disk, preferably radio quiet like the region of minimum sky brightness at ($\delta = +35, \alpha = 9^h 30^m$);

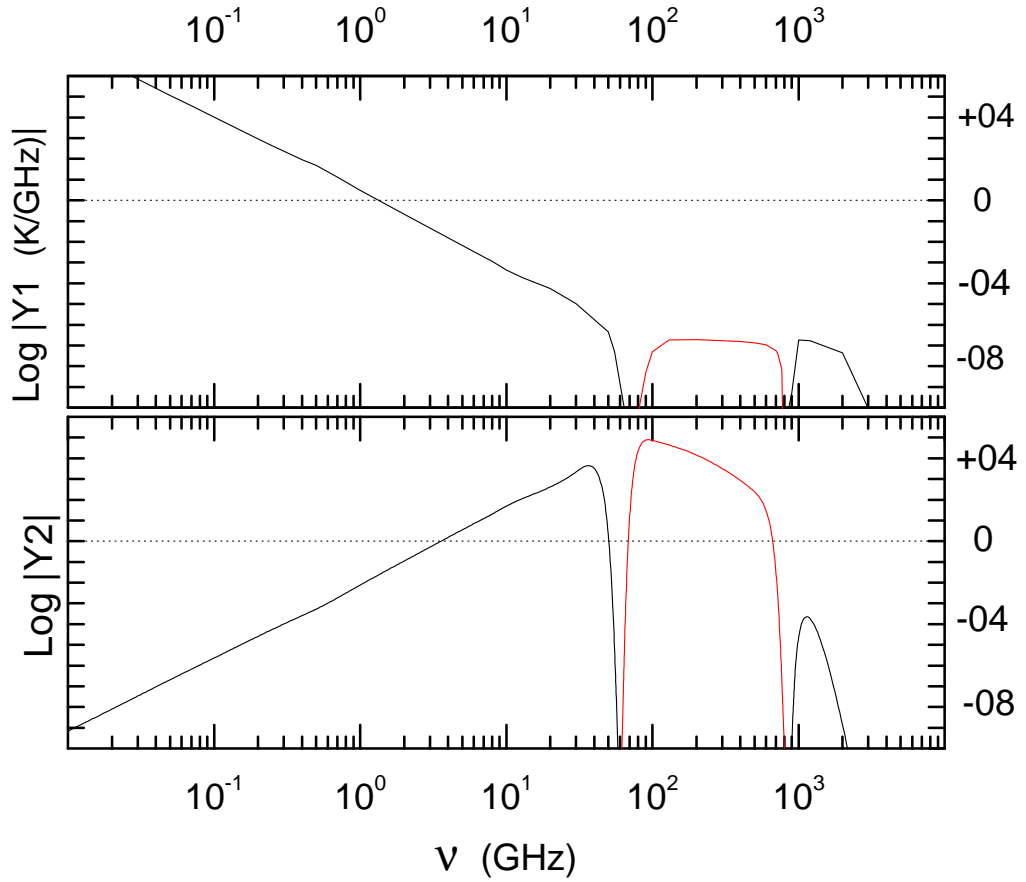


Figure 5. Average behaviour of $Y1 = dT_{for}/d\nu$ vs ν (upper panel) and $Y2 = \Delta T_b^{CMB}/\Delta T_{for}$ vs ν (lower panel). For a better appreciation of the variations of $Y1$ and $Y2$ Log scales have been used and absolute values of $Y1$ and $Y2$ plotted (negative values of $Y1$ and $Y2$ marked in red). The change of sign of $\Delta T_b^{CMB}/\Delta T_{for}$ around 70 GHz is a consequence of the fact that above that frequency the dust signal overcomes the synchrotron (see fig.2). Plotted values and profiles are typical values. The effective values depend on the observing direction (galactic foregrounds are anisotropically distributed and combine in different ways).

iv)observing site:

- in space: far from Earth and Sun (e.g. L2 point)
- on Earth ground: at special sites, (high altitude, dry, isolated radioprotected sites), like the Antarctic Plateau during the local winter or the Atacama Desert, for observation of southern sky regions, White Mt. and, at frequencies below few GHz, where atmospheric absorption is small also at low altitudes, Green Bank, for studies of northern sky regions.

Space and Antarctica are preferable because their environment conditions are particularly stable and contribute to get low values of T_{sys} , the *system noise temperature*. The *minimum detectable signal*, (1σ), is in fact

$$T_{min} = k_s \frac{T_{sys}}{\sqrt{\Delta\nu \tau}} \quad (4.7)$$

where $\Delta\nu$ is the system bandwidth, $\tau = n\tau_o$ the integration time, n the number of independent observations of the same area of sky, τ_o the system time constant, k_s a system constant close to

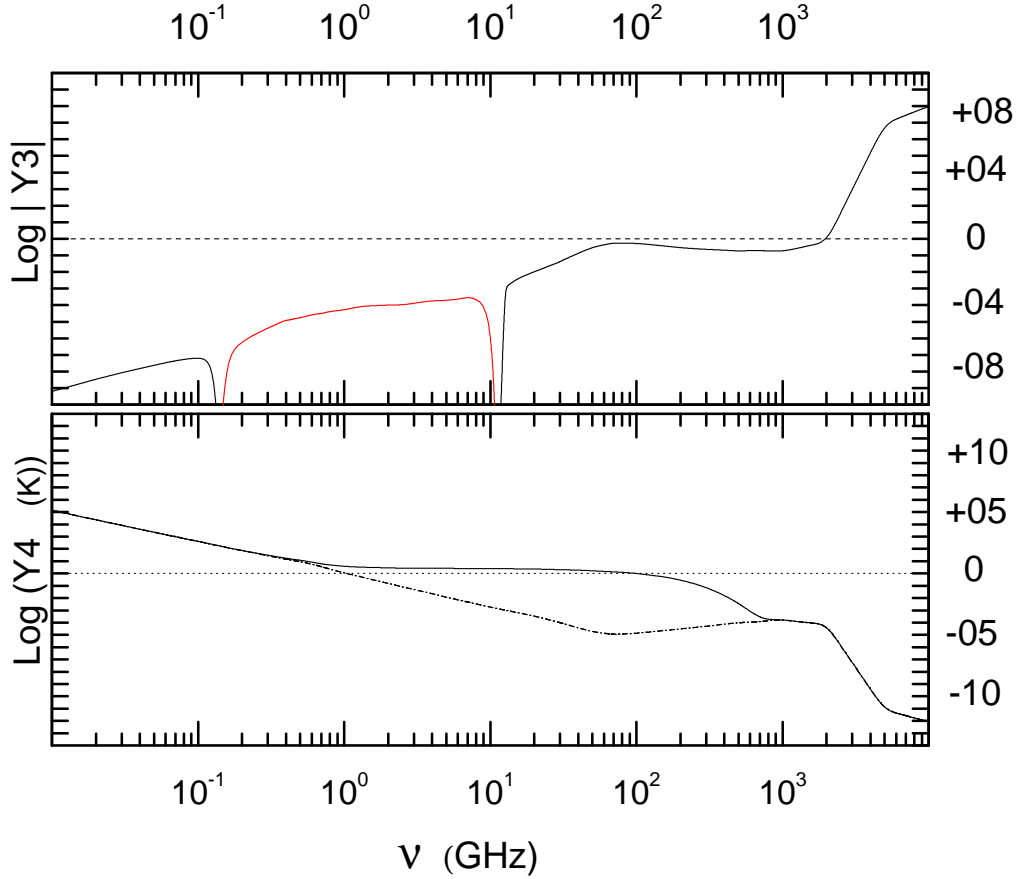


Figure 6. Average behaviour of $Y3 = \delta(\nu)/(T_{for} + T_b^{CMB})$ vs ν (upper panel) and $Y4 = T_{for} + T_b^{CMB}$ vs ν (lower panel) where δ is the spectral distortion (see eq. 2.1) of a Bose Einstein distortion with the amplitude profile shown in fig.1 and maximum deviation from the undistorted spectrum of $+/- 10^{-4}$ K. For a better appreciation of the variations of Y3 and Y4 Log scales have been used and absolute values of Y3 and Y4 plotted (negative values of Y3 marked red). The effective values and trend of Y3 and Y4 one can expect to observe at a given site can be more subtle and intricate because the foregrounds are anisotropically distributed and different types of CMB distortions are probably present.

1 whose value depends on the shape of the system bandwidth and the receiver configuration. If $\Delta\nu = \beta\nu$ eq.(4.7) gives:

$$\left[\frac{\Delta T}{\delta\nu} \right]_{min} \simeq \frac{dT_{min}}{d\nu} = \frac{k_s \beta \tau}{2} \frac{T_{sys}}{(\beta\nu \tau)^{3/2}} = \frac{T_{min}}{2\nu} \quad (4.8)$$

v)prefer digital or digitally controlled subsystems (for quick adjustments of the system configuration if unforeseen effects appear);

vi)include a reference source, preferably a blackbody of temperature T_o , close to the sky temperature. The value of T_o can be poorly known but its stability must be very high ($\Delta T/T \leq 10^{-6}$ over a complete observing period);

vii) for helping to recognize foreground signals, the capability of measuring linear polarization of the signal is desirable.

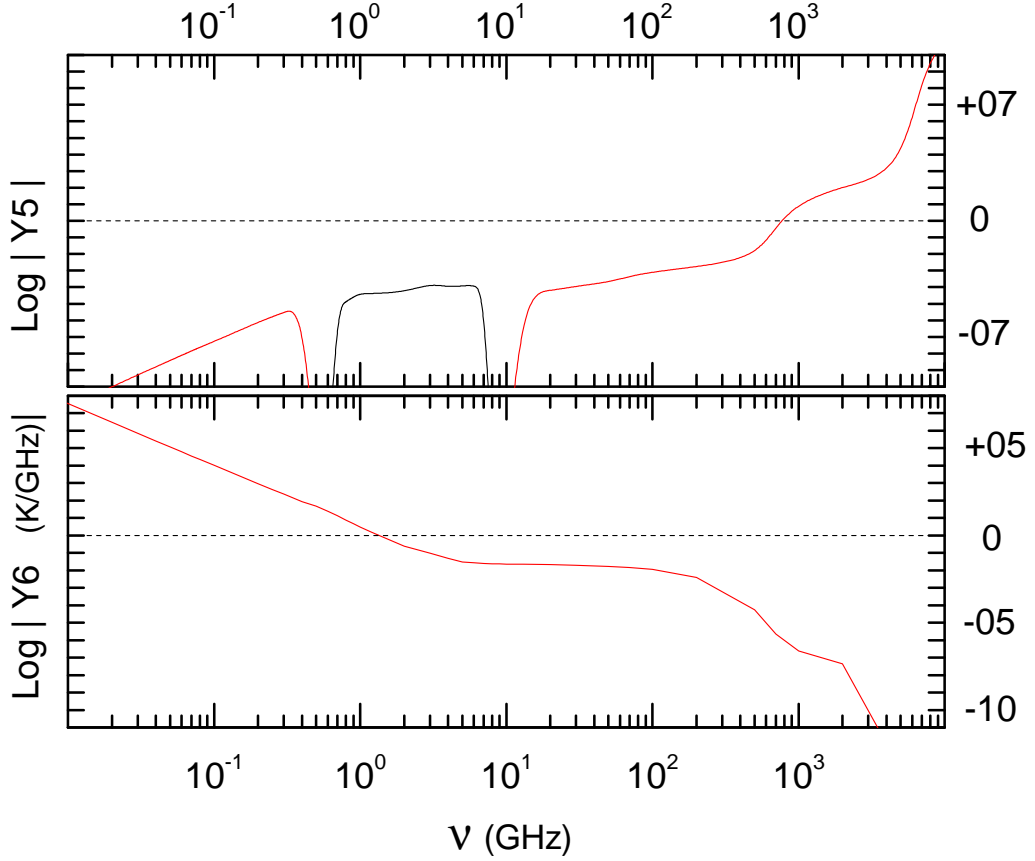


Figure 7. Average behaviour of $Y5 = |\Delta(\delta(\nu))/\Delta(T_{for} + T_b^{CMB})|$ vs ν (upper panel) and $Y6 = d(T_{for} + T_b^{CMB})/d\nu$ vs ν (lower panel) for the same Bose Einstein distortion of fig.6. Comments to the caption of fig.6 hold also here

4.6 Practical system configurations

Different configurations are possible, for instance the one shown in fig.8. The choice among them depends on the frequency region of the CMB spectrum to be explored, the technology available and the observing site. Whatever the choice will be all the configurations must include the following subsystems:

i) *Radiation Collector (RC).*

It must collect the sky signal through a frequency independent, well shaped circular beam, and split it in two orthogonal, linearly polarized components. Beam shape and levels of side- and back- lobes must be carefully measured before observation, at a level accuracy of least -60dB. At high frequencies RC can be a Concentrator (see for instance [30]), at low frequencies an under illuminated parabola. In both cases the typical aperture dimension is

$$D \simeq 60 \frac{\lambda}{\Delta\theta_o} \quad (4.9)$$

where λ is the maximum wavelength and $\Delta\theta_o$ the system angular resolution ($D \sim 12\lambda$ for $\theta = 5^\circ$).

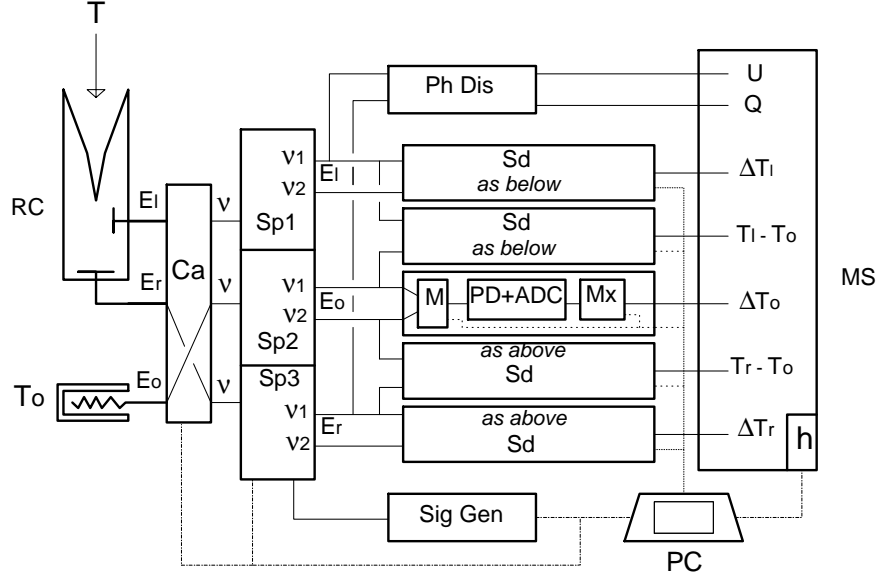


Figure 8. Block Diagram of a possible configuration of a system for measurements of the CMB spectral distortions. T = sky temperature, RC = radiation collector, To = dummy load, Ca = front end multiple switch, SPi = two channel spectrometer, Sd = synchronous detector, M = modulator, PD = power detector, ADC = analog to digital converter, Mx = multiplier, SigGen = high frequency signal generator, PhDis = phase discriminator, MS = mass storage, PC = system control, Ei & Er = signals produced by the left & right polarized components of the incoming signal, Eo = dummy load signal, U & Q = Stokes parameter of the sky signal, $\Delta T_i = T_i(\nu_1) - T_i(\nu_2)$, h = housekeeping and auxiliary data (ν, ν_1, ν_2 , time, beam position ...).

It sets the dimension of the RC aperture. Because the CMB is a monopole the search of CMB distortions would not require a particular beam aperture where not for the foregrounds and environment signal. The great majority of the studies of the CMB spectrum so far made used beamwidths ranging between few (angular) degrees and 15° .

As eq.4.9 shows large beams mean antennae/radiation collectors of small aperture. Usually simple and cheap it can be easily installed in space or at ground observatories, and smooth sky irregularities inside the antenna field of view. But the sky area to be mapped for foreground studies becomes large so finding regions with regular distribution and minimum values of the foregrounds may be difficult.

Small and very small beams on the contrary mean antennae of large apertures, usually expensive and difficult to install on a space vehicle. They reduce the extension of sky region to be mapped but make the radiometer more sensitive to compact sources and foreground irregularities.

For completely new experiments, because we want to observe also at frequencies below 1 GHz, $\Delta\theta_o \simeq 5^\circ$ is a reasonable trade off but if there are opportunities of using already

existing systems beamwidths between 1° and 5° can be accepted.

ii) *Stable Thermal Reference Source* (T_o): a dummy load, temperature stabilized by a bath of boiling liquid with boiling temperature as close as possible to the sky temperature (Helium between 1 and 600 GHz, Argon or Nitrogen at other frequencies). For maximum stability of the load effective temperature the level of the liquid must be kept constant by automatic refilling system;

iii) *Signal Generator* (SigGen)

Digitally controlled set the central frequency of observations and moves it in steps of amplitude $\Delta\nu_o$ over the frequency region to be explored;

iv) *Two Channel Spectrometer* (Sp).

Driven by the Signal Generator and fed by RC or T_o provides for each frequency ν two outputs, the sky signals at $\nu_1 = \nu - \Delta\nu/2$ and $\nu_2 = \nu + \Delta\nu/2$ ($\Delta\nu/\nu \simeq 0.1$ and $\delta\nu_i/\nu_i \simeq 0.03$) where $\Delta\nu \simeq \Delta\nu_o/3$ and $\delta\nu$ are respectively the frequency separation of the signals and the spectrometer frequency resolution. Sp can be a combination of transmission lines and/or omo- or ethero-dyne radiofrequency systems at low frequencies (region R1), quasi optical and optical systems at high and very high frequencies (regions R2 and R3);

v) *Synchronous detectors* (Sd). Evolution of the classical Dicke receiver (see for instance [54]), includes Modulator (M), Power Detector (Pd) and Multiplier (Mx)). Its output is the difference between the signals at frequency ν_1 and ν_2 which arrive from Sp;

vi) *Power Detector* (PD): cooled bolometer (preferred) or etherodyne receiver (with diodes and low noise preamplifiers), gives an output proportional to the power associated to the incoming signal;

vii) *Analog to Digital Converter* (ADC): installed as close as possible to the Radiation Collector, for maximum flexibility of system configuration;

viii) *Phase Discriminator* (PhD): evaluates the Stokes Parameters (U and Q or V and Q depending on the polarization type of the the Radiation Collector outputs, (see for instance MIPOL [55], SPORt ([56]) and references therein);

ix) *Multiple Switch* (Ca): for swapping the spectrometer inputs and detecting systematic effects;

x) *Mass Storage* (MS): digital repository of all the measured quantities, plus time, frequencies ν, ν_1, ν_2 , system configuration and housekeeping data;

xi) *Control Unit*(PC): drives all the subsystems and data recording system.

Subsystems ahead of the ADC converters are analogic units digitally controlled by the system control unit. Subsystems which follow the ADC converters are digital units realized via software which can be reconfigured whenever necessary. Therefore closer the ADC units are to the system front end, more flexible the system is.

To minimize T_{sys} , reduce T_{min} and increase the system sensitivity, RC and front end components must be cooled to a temperature close to the sky temperature.

To check the efficiency of the differential system and its capability of detecting with 1% accuracies distortions of minimum amplitude 10^{-a}

i) the effective temperature T_o^{eff} of the dummy load measured at the input of each of the two channel spectrometers Sp_i must be stable at the level of a part on $10^{(a+2)}$ over the entire observing period and have a known frequency dependence with maximum variation of a part on $10^{(a+2)}$ over $\Delta\nu = \nu_2 - \nu_1$, the frequency separation of the Sp outputs;

ii) at each frequency ν the difference between the two outputs of Sp_i , when the spectrometer is fed by the dummy load, must be less than a part on $10^{(a+2)}$.

For instance for a 10^{-6} minimum detectable distortion, ($a = 6$), the dummy load effective temperature must be stable to a part on 10^8 while an integration time of 11 day per sky bin will be necessary to allow the detection at 1σ c.l. of distortion of absolute amplitude $\geq 10^{-6}$.

The absolute value of T_o^{eff} does not affect the measurements of ΔT_i over the frequency region (e.g. R1 or R2 or R3) explored by one radiometer, but can help to link results obtained by different radiometers and/or observers operating in the same or in a different frequency region.

Calibration of the system response (adc units/K) can be made (in laboratory and possibly also at the observing site or platform) feeding each Sp_i with the dummy load, and pumping on the bath of the boiling liquid to change its temperature by a known quantity and measuring the variation of the signals at each of the Sp_i outputs.

5 Perspectives of new searches of CMB spectral distortions

As already said the differential approach does not improve nor worsen the evaluation of the foreground contributions but makes the accuracies of all the measured quantities independent from the zero level of the scales of temperature and less prone to systematic effects than absolute measurements. Accuracies of a part on 10^6 or better are therefore possible.

To solve completely the puzzle of the CMB distortions at least three systems, covering frequency region R1, R2 and R3 respectively, are necessary (see fig.2):

In Region 1, ((0.3 - 30) GHz),
 - below 3 GHz (Region R1a) an underilluminated curved reflector of radius $R = 12$ m or more is necessary, fed by a system of dipoles or by a concentrator, arranged in such a way to produce a frequency independent beam with $\Delta\theta_o \simeq 5^\circ$. This will leave on the reflector an unused external rim, $\sim (R - (60/\Delta\theta_o)\lambda)$ which will act as a screen against undesired signals. This reflector aperture makes impossible observations using rockets and balloons and requires deployable systems if we decide for satellites. Sp can be made using classical radioastronomical techniques (combinations of transmission lines and/or omo- or etherodyne systems). Power detection by Diodes fed by low noise amplifiers will be used until good, cooled, bolometers will become available also at low frequencies.

- above 3 GHz (Region R1b) small dimensions of RC and other system components make observations from stratospheric balloons or even better in space, where environment contamination is practically absent, more appealing. Cooled bolometers can be used for detection.

In Region 2 , ((30 - 600) GHz) atmospheric absorption makes ground observations impossible, except in two windows at about 30 and 90 GHz, and disturbs balloon experiments. Observations therefore must be made in space using satellites which must accommodate radiation collectors with a maximum aperture of 1.2 m and compact subsystems based on microwave and IR techniques. Rockets can be used only for radiometer operating at frequencies ≥ 100 GHz, where the maximum aperture of the radiation collector is 4 cm.

Radiation Collector (RC)	<ul style="list-style-type: none"> - curved reflector - diameter 12 m - steerable along the meridian - cryogenically cooled concentrator/illuminator - ground screen
Beam	<ul style="list-style-type: none"> - frequency independent - HPBW = 5° - side lobes and back lobes < -60 dB
Receiver (Rx)	<ul style="list-style-type: none"> - triple differential radiometer - cryogenically cooled between RC and power detectors - polarization sensitive - digitally controlled - $T_{sys} \lesssim 10K$ - operation frequencies = 0.3 – 30 GHz
Reference Source (T_o)	<ul style="list-style-type: none"> - criogenically cooled dummy load (see text) - effective temperature accuracy: 1% - stability $\Delta T_o/T_o \leq 10^{-6}$ during the transit through the antenna beam of a pointlike source
Two Channel spectrometers (Sp)	<ul style="list-style-type: none"> - frequency separation of the two channels $\Delta\nu/\nu = 0.1$ - frequency resolution $\delta\nu/\nu = 0.03$
Observation	<ul style="list-style-type: none"> - at Dome C or Amundsen Scott base (Antarctica) - transit mode, at nighttime - repeated at different declinations
Expected sensitivity	<ul style="list-style-type: none"> - $[\frac{\Delta T}{\delta\nu}]_{min} \lesssim 10^{-12}$ K/Hz
Integration time	<ul style="list-style-type: none"> - ≤ 5 d/sky bin ($T_{min} = 5 \cdot 10^{-6}$ K , 1σ) - ≤ 1.2 d/sky bin ($T_{min} = 10^{-5}$ K , 1σ)

Table 1. Expected Characteristics of LFGDR (Low Frequency Ground Differential Radiometer) for the search of CMB spectral distortions at low frequencies from Antarctica (see text and fig.3)

Detection and dispersion systems can be mixtures of microwave and IR techniques.

In Region 3 ($\nu > 600$ GHz) only rockets and satellites offer a possibility of carrying on observations, accommodating systems more and more compact, similar to optical radiometers with cooled bolometers for detection and IR derived dispersion systems.

6 Conclusions

The best observing conditions can be found in space, especially at distant sites like point L2, where quiet and stable environment conditions minimize the system noise and guarantees optimum observing conditions. But: i)preparing a system for operation in space is very expensive, ii)there are long waiting lists of space projects, already approved and waiting to be launched or in the approval phase. 1

1We cannot reasonably expect that newly proposed experiments, if accepted, will fly before 2030-2040, so to be practical and to keep our feet on the ground:

- for Regions R2 and R3 we can think about the possibility of becoming part of more ambitious space and balloons experiments already proposed for measurements of the CMB polarization, among them PIXIE [57], PRISM [58], LSPE [59] and their evolutions.

Generally they have narrow beams and plan to explore the whole sky, characteristics which are not necessary for the search of CMB spectral distortions, but useful to improve our knowledge of the foregrounds. If these experiments will be adapted or already include continuous frequency coverage and on board evaluation of the frequency derivative of the sky signal probably besides polarization will detect also CMB spectral distortions.

- for Region R1 after LOBO [60–62] and DIMES [63] apparently no other proposals for the search of CMB distortions at frequencies below few GHz have been submitted to the funding agencies nor can be found in literature. Because at these frequencies the dimensions of the radiation collector, (~ 12 m for 5° angular resolution), is definitely too large for balloons and rockets, ground based observations from the Antarctic Plateau or from the Atacama desert are the only possibility if we want to carry on observation before the end of the next decade. To operate in the very harsh environment existing there it will be necessary to get support at the Amundsen Scott base at South Pole ([64]), or even better at Dome Concordia Station [65] for Antarctica or from ALMA [66] at Atacama. Let's call this experiment LFGDR (Low Frequency Ground Differential Radiometer) (see Table 2).

But if we can wait and ready to plan experiments in Region 1 also from space (let's call it LFSDR, Low Frequency Space Differential Radiometer) deployable curved reflectors have to be considered.

Studies of deployable (e.g. [67]) and ground based (e.g. [60]) reflectors for observation of CMB and diffuse galactic emission have been made in the past and large reflectors for other radioastronomical observations have been already sent and deployed in space(e.g. [68]).

The need of using a 12 m class reflector will make LFSDR so huge and expensive that, if approved and supported, will probably accommodate as piggy back also the systems for the search of CMB distortions in regions R2 and R3.

Whatever will be the future, it is necessary to begin immediately ancillary systematic observations of the foregrounds using already existing radiotelescopes and start technological studies for improving many radiometer components. Among them:

- i) optimum geometry of (parabolic or spherical) reflectors with small f number, illuminators and concentrators,
- ii) cooled illuminators/concentrators
- iii) low noise, low frequency, bolometers ,
- iv) tunable, two outputs, frequency spectrometers,
- v) stable, low temperature noise sources
- vi) fast ADC system operating, at the highest frequencies,
- vii) digitization of all subsystems at all the frequencies.

A list of operations which will keep us busy for years, with important outcomes also for other type of research, to be carried anyway.

Acknowledgments

I thanks J.Peebles and the organizers of CMB@50 (Princeton, June 2015) for inviting me to give a talk on perspective of detecting CMB spectral distortions, which triggered me, when I came back, to put it in written form . I am indebted to Massimo Gervasi, Mario Zannoni and Enrico Pagana for many discussions, and hope they will have the opportunity, I lost because of retirement, of detecting CMB distortions.

References

- [1] Penzias A.A., Wilson R.W., *A Measurement of Excess Antenna Temperature at 4080 Mc/s.*, *ApJ* **142** (1965) pg. 419-421.
- [2] Mather J.C. et al., *A preliminary measurement of the cosmic microwave background spectrum by the Cosmic Explorer (COBE) satellite*, *ApJ* **354L** (1290) pg. 37-40
- [3] Fixsen D.J *The Temperature of the Cosmic Microwave Background*, *ApJ* **707** (2009) pg.916-920
- [4] Partridge R.B., *3K: The Cosmic Microwave Background Radiation*, Cambridge University Press (1995).
- [5] Longair M., *High Energy Astrophysics*, Cambridge University Press (2011)
- [6] Sunyaev R.A., Zeldovich Ya.B. *The spectrum of primordial radiation, its distortions and their Significance* , *CoASP* **2** (1970) pg. 66-74.
- [7] Danese L, De Zotti G.F., *The relic radiation spectrum and the thermal history of the Universe* , *Riv. Nuovo Cimento* **7** (1977) pg. 277-362.
- [8] Daly R.A. , *Spectral distortions of the microwave background radiation resulting from the damping of pressure waves*, *ApJ* **371** (1991) pg. 14-28.
- [9] Chluba J., Sunyaev R.A., *The evolution of CMB spectral distortions in the early Universe*, *MNRAS* **419** (2012) pg. 1294-1314.
- [10] De Zotti G., Negrello M., Castex G., Lapi A., Bonato M., *Another look at distortions of the Cosmic Microwave Background spectrum*, arXiv:512.04816v2, 9 Feb 2016
- [11] Chluba J., Sunyaev R.A., *Pre-recombinational energy release and narrow features in the CMB spectrum*, *A&A* **501** (2009) pg. 29-47
- [12] <http://www.rri.in/DISTORTION/apsera.html>
- [13] Ade P.A.R. et al. *Planck 2013 results. I. Overview of products and scientific results*, *A&A* **571** (2014) 1-32.
- [14] Ansari . et al., *21 cm observation of LSS at $Z \sim 1$. Instrument sensitivity and foreground subtraction* arXiv:1108.1474v1, 6 August 2011
- [15] Beck R., Wielebinski R., *Magnetic Fields in Galaxies, Planets, Stars and Stellar Systems* **5** chapt.13 (2013), Springer, Berlin
- [16] Liu A., Pritchard J.R., Tegmark M., Loeb A. *Global 21 cm signal experiments: A designer Guide*, *PRD* **87** (2013) 043002-1 - 043002-31.
- [17] Furlanetto S.R. et al. *Astrophysics from the Highly-Redshifted 21 cm line*, *Astro2010 Decadal Survey Science Frontier Panel: Galaxies across Cosmic time* (submitted) (2010) .
- [18] Zannoni M. et al., *TRIS I. Absolute Measurements of the Sky Brightness Temperature at 0.6, 0.82 and 2.5 GHz*, *ApJ* **688** (2008) pg. 12-23.
- [19] Gervasi M., Zannoni M., Tartari A., Boella G., Sironi G., *TRIS II. Search for CMB Distortions at 0.60, 0.82 and 2.5 GHz*, *ApJ* **688** (2008) pg. 24-31.

- [20] Stankevich K.S., Wielebinski R., Wilson W.E. , *Radio sky background studies using the Moon as a screen*, *AuJPh* **23** (1970) pg. 529-539
- [21] Salvaterra R., Burigana C., *Construction of a Database of CMB Spectrum Observations* , arxiv: astro-ph/0206350
- [22] Smoot G.F. et al., *Low Frequency Measurements of the Cosmic Background Radiation Spectrum*, *ApJ* **291** (1985) pg. L23-L27.
- [23] Bersanelli M. et al., *Absolute measurements of the cosmic microwave background from the Amundsen-Scott South Pole Station, Antarctic J.* **XXVIII** (1993) pg. 306-308.
- [24] Fixsen D.J. et al., *ARCADE2 Measurement of the Absolute Sky Brightness at 3-90 GHz*, *ApJ* **734** (2011) pg. 1-11.
- [25] Fixsen D.J. et al., *The Cosmic Microwave Background Spectrum from the full COBE FIRAS Data Set* , *ApJ* **473** (1996) pg. 576-587
- [26] Gush H.P., Halpern M., Wishnow E.H, *Rocket easurement of the cosmic-background-radiation mm-wave spectrum*, *PhR Lett.* **65** (1990) pg. 537-540.
- [27] Partridge R. et al., *Automated measurement of the temperature of the atmosphere at 3.2 cm*, *PhysRev.D* **29** (1984) pg. 2683-2685.
- [28] Tartari A., Zannoni M., Gervasi M., Boella G., ironi G., *TRIS III. The Diffuse Galactic Radio Emission at $\delta=+4^\circ$* , *ApJ* **688** (2008) pg. 32-42.
- [29] Howell T.F., Shakeshaft J.R., *Spectrum of the 3° K Cosmic Microwave Radiation*, *Nature* **216** (1967) pg. 753-754.
- [30] Mather J.C., Fixsen D.J., Shafer R.A., *Design for the COBE Far Infrared Absolute Spectrophotometer (FIRAS)*, *Proc SPIE* **2019** (1994) pg. 168-179.
- [31] Sironi G, Boella G., Gervasi M., Tartari A., Zannoni M., *The CMB spectrum: Perspective of observing spectral distortions*, *New. Ast. Rev.* **51** (2007) pg.406-410
- [32] Ajello C., Bonelli G., Sironi G., *Evaluation of the Earth's Atmospheric Brightness Temperature at Decimetric Wavelengths* **ApJ Supp.**(96) pg. 643-650.
- [33] Sironi G., *The Spectrum of the Galactic Non-Thermal Background Radiation-I. Observations at 151.5 and 408 MHz*, *MNRAS* **166** (1974) pg. 345-353.
- [34] Strong A.W., Orlando E. and Jaffe T.R. *The interstellar cosmic-ray electron spectrum from synchrotron radiation and direct measurements*, *A&A* **534** A54(2011) pg. 1-13.
- [35] Aguilar M. et al, *Precision easurements of the $e^+ + e^-$ flux of primary cosmic ray electrons from 0.5 GeV to 1 TeV with AMS on ISSA*, *PhRvL* **113** (2014) 221102.
- [36] Tartari A. et al., *On the detectability of cosmic ray electron spectral features in the microwave/mm-wave range*, *Proc.12th ICATPP Conf.* **6** (2010) pg. 58-65 ISBN 978.981-4329-02-6.
- [37] Berkhuijsen E.M., *A Survey of the Continuum Radiation at 820 MHz between Declinations -7° and $+85^\circ$* , *A&A* **14** (1971) pg. 359-386
- [38] Bernardi G. et asl., *Polarization Observations in a Low Synchrotron Emission Field at 1.4 GHz* , *ApJ* **594** (2003) pg. L5-L8.
- [39] Gervasi M., Tartari A., Zannoni M., Boella G., Sironi G., *The Contribution of the Unresolved Extragalactic Radio Sources to the Brightness Temperature of the Sky* *ApJ* **682** (2008) pg. 223-230.
- [40] Albergel A. et al, *Planck 2013 results. XI. All-sky model of thermal dust emission* , *A&A* **571** (2014) A11 pg. 01-37.

- [41] Ade P.R. et al., *Planck Intermediate Results XXII. Frequency dependence of thermal emission from Galactic dust in intensity and polarization*, arxiv:1405.0874
- [42] Kogut A. *Anomalous Microwave Emission*, <https://cds.cern.ch/record/379836/files/9902307.pdf>.
- [43] Dickinson C. *PRISM (A study of Anomalous Microwave Emission (AME) in Galactic Clouds with Planck*, <http://www.rssd.esa.int/.../47> ESLAB April 04 11 55.
- [44] Dame T.M., Hartmann D. and Thaddeus P., *The Milky Way in molecular clouds: a new complete CO survey*, *ApJ* **547** (2001) pg. 792-813.
- [45] Landecker T.L., Wielebinski R., *151 MHz all-sky Continuum Survey*, *AuJPh.Suppl.* **47** (1970) pg. 1-20
- [46] Haslam C.G.T., Salter C.J., Stoffel H., Wilson W.E., *A 408 MHz all-sky Continuum Survey II. The Atlas of Contours Maps*, *A&A Suppl.* **47** (1982) pg. 1-143.
- [47] Remazeilles M., Dickinson C., Bandy A.J., Bigot-Sazy M.A., Ghosh T., *An improved source-subtracted and destriped 408 MHz all-sky map*, arxiv:1411-3268.
- [48] Calabretta M.R., Staveley-Smith L., Barney D.G., *A New 1.4 GHz Radio Continuum Map of the Sky South of Declination + 25°*, *PASA* **31** (2014) pg. e7-35.
- [49] Adam P. et al, *Planck 2015. Diffuse component separation. Foreground maps*, arXiv 1502.01588.
- [50] Zheng H., Tegmark M., Dillon J.S., Liu A., Neben A.R., Jonas J., Reich. P. and Reich W. , *An improved model of diffuse galactic radio emission from 10 MHz to 5 THz*, arXiv:1605.04920v1 16 May 2016
- [51] Jarosik N. et al., *Severn Years Wilkinson Microwave Anisotropy Probe (WMAP) Observations: Sky maps, Systematic Errors and Basic Results*, *ApJS* **192** (2011) pg. 14-29.
- [52] Ade P.A.R. et al., *BICEP2 I: Detection of B mode Polarization at Degree Angular Scales*, *PhR Lett* 112.241101 (2014).
- [53] Haslam C.G., Large M., Quigley M.F., *A Radio Study of the North Polar Spur*, *MNRAS* **127** (1963) pg. 273-285.
- [54] Krauss J.D., *Radio Astronomy*, Mc Graw Hill (1966) pag.248-254
- [55] Gervasi M. et al., *Dual output polarimeter devoted to the study of the Cosmic Microwave Background*, *Proc of SPIE* **4843** (2003) pg. 336-347.
- [56] Carretti E. et al., *SPOrt: an Experiment Aimed at Measuring the Large Scale Cosmic Microwave Background Polarization*, *Proc. SPIE* **4843** (2003) pg. 305-307.
- [57] Kogut A. et al., *The Primordial Inflation Explorer (PIXIE): A Nulling Polarimeter for Cosmic Background Observations* *JCAP* **2011** (2011) pg. 07-025.
- [58] Andre' P. et al, *PRISM (Polarized Radiation Imaging and Spectroscopy Mission): an extended white paper*, *JCAP* **2014** (2014) pg. 02-06.
- [59] Aiola ert al., *The Large Scale Polarization Explorer (LSPE)*,*Proc.SPIE* **84467A** (2012) pg. 1-20.
- [60] Sironi G., Bonelli G., Dall' Oglia G., Pagana E., De Angeli S., Perelli M. *Measurements of the CBR Frequency Spectrum at Low Frequencies: Ground and Space Observations* , *ApL&C* **32** (1995) pg. 31-36.
- [61] Pagana E., Perelli M. *Low Frequency Background Observatory (LOBO) Feasibility Study*, *FPM Space srl and IMT(1993) F.P.M.07/93/SDA*.
- [62] Sironi G., Bonelli G. *LOBO (LOW frequency Background Observatory)*, *Proc. SDmall Mission Opportunities and the Scienmtific Community - Colleferro(Rome)***2** (1995) pg. 69-73.

- [63] Kogut A. , *Diffuse Microwave Emission Survey*, arxiv:astro-ph/9607100
- [64] <https://www.nsf.gov/geo/plr/support/southp.jsp>
- [65] <http://www.italiantartide.it/>
- [66] <http://www.almaobservatory.org/>
- [67] Bernasconi M.C., Pagana E., Reibald G.G, *Large Inflatable Space-Rigidized Antenna Reflectors, Proc. 38th Cong. Int. Astronautical Fed. IAF-87* (1987) pg. 315.
- [68] <http://www.vsop.isas.jaxa.jp/obs/news/www.161.html>